Afshar Vahid, Shahraam; Warren-Smith, Stephen; Monro, Tanya Mary.
Enhancement of fluorescence-based sensing using microstructured optical fibres, *Optics Express*, 2007; 15 (26):17891-17901.

Enhancement of fluorescence-based sensing using microstructured optical fibres

Shahraam Afshar V., Stephen C. Warren-Smith and Tanya M. Monro

Centre of Expertise in Photonics, School of Chemistry & Physics, University of Adelaide, Adelaide, SA 5005, Australia

shahraam.afshar@adelaide.edu.au

Abstract: We develop a generic model of excitation and fluorescence recapturing within filled microstructured optical fibres (MOFs) with arbitrary structure and demonstrate that the light-matter overlap alone does not determine the optimal fibre choice. Fibre designs with sub-wavelength features and high-index glasses exhibit localised regions of high intensity, and we show that these regions can lead to approximately two orders of magnitude enhancement of fluorescence recapturing. Here we show how this regime can be exploited for sensing and demonstrate experimentally in-fibre excitation and fluorescence recapturing within a filled, solid-core MOF.

OCIS codes: (060.2370) fiber optics sensors; (060.4005) microstructured fibers; (280.1415) biological sensing and sensors

References and links

1. G. Stewart and B. Culshaw, "Optical Waveguide Modelling and Design for Evanescent Field Chemical Sensors," Opt. Quantum Electron. **26**, s249 (1994).
2. J. B. Jensen, P. E. Hoiby, G. Emiliyanov, O. Bang, L. H. Pedersen, and A. Bjarklev, "Selective Detection of Antibodies in Microstructured Polymer Optical Fibers," Opt. Express **13**, 5883–5889 (2005).
3. S. O. Konorov, A. M. Zheltikov, and M. Scalora, "Photonic-Crystal Fiber as a Multifunctional Optical Sensor and Sample Collector," Opt. Express **13**, 3454–3459 (2005).
4. L. Rindorf, P. E. Hoiby, J. B. Jensen, L. H. Pedersen, O. Bang, and O. Geschke, "Towards Biochips Using Microstructured Optical Fiber Sensors," Anal. Bioanal. Chem. **385**, 1370–1375 (2006).
5. C. M. B. Cordeiro, M. A. R. Franco, G. Chesini, E. C. S. Barretto, R. Lwin, C. H. B. Cruz, and M. C. J. Large, "Microstructured-Core Optical Fibre for Evanescent Sensing Applications," Opt. Express **14**, 13,056–13,066 (2006).
6. F. Warken, E. Vetsch, D. Meachede, M. Sokolowski, and A. Rauschenbeutel, "Ultra-Sensitive Surface Absorption Spectroscopy Using Sub-Wavelength Diameter Optical Fibers," Opt. Express **15**, 11,952–11,958 (2007).
7. S. Smolka, M. Barth, and O. Benson, "Highly Efficient Fluorescence Sensing with Hollow Core Photonic Crystal Fibers," Opt. Express **15**, 12,783 (2007).
8. W. Henry, "Evanescent Field Devices: A Comparison Between Tapered Optical Fibres and Polished or D-Fibres," Opt. Quantum Electron. **26**, s261–s272 (1994).
9. P. Lucas, M. R. Riley, C. Boussard-Pledel, and B. Bureau, "Advances in Chalcogenide Fiber Evanescent Wave Biochemical Sensing," Anal. Biochem. **351**, 1–10 (2006).
10. G. Stewart, W. Jin, and B. Culshaw, "Prospects for Fibre-Optic Evanescent-Field Gas Sensors Using Absorption in the Near-Infrared," Sens. Actuators B **38-39**, 42–47 (1997).
11. J. Lou, L. Tong, and Z. Ye, "Modeling of Silica Nanowires for Optical Sensing," Opt. Express **13**, 2135–2140 (2005).
12. Y. Zhu, H. Du, and R. Bise, "Design of Solid-Core Microstructured Optical Fiber with Steering-Wheel Air Cladding for Optimal Evanescent-Field Sensing," Opt. Express **14**, 3541–3546 (2006).

13. J. B. Jensen, L. H. Pedersen, P. E. Hoiby, L. B. Nielsen, T. P. Hansen, J. R. Folkenberg, J. Riishede, D. Noordegraaf, K. Nielsen, A. Carlsen, and A. Bjarklev, "Photonic Crystal Fiber Based Evanescent-Wave Sensor for Detection of Biomolecules in Aqueous Solutions," Opt. Lett. **29**, 1974–1976 (2004).
14. Y. K. Lize, E. Magi, V. Taeed, J. Bolger, P. Steinvurzel, and B. Eggleton, "Microstructured Optical Fiber Photonic Wires with Subwavelength Core Diameter," Opt. Express **12**, 3209–3217 (2004).
15. K. J. Rowland, S. Afshar V., and T. M. Monro, "Nonlinearity Enhancement of Filled Microstructured Fibers Operating in Nanowire Regime," in *Proceedings of OFC 2006*, p. OTuH3 (2006).
16. L. Tong, J. Lou, and E. Mazur, "Single-Mode Guiding Properties of Subwavelength-Diameter Silica and Silicon Wire Waveguides," Opt. Express **12**, 1025–1035 (2004).
17. S. Smolka, M. Barth, and O. Benson, "Selectively Coated Photonic Crystal Fiber for Highly Sensitive Fluorescence Detection," Appl. Phys. Lett. **90**, 111,101 (2007).
18. Z. Liu and J. Pawliszyn, "Capillary Isoelectric Focusing of Proteins with Liquid Core Waveguide Laser-Induced Fluorescence Whole Column Imaging Detection," Anal. Chem. **75**, 4887–4894 (2003).
19. Y. Huang, Y. Xu, and A. Yariv, "Fabrication of Functional Microstructured Optical Fibers Through a Selective-Filling Technique," Appl. Phys. Lett. **85**, 5182 (2004).
20. T. Ritari, J. Tuominen, H. Ludvigsen, J. Petersen, T. Sorensen, T. Hansen, and H. Simonsen, "Gas Sensing Using Air-Guiding Photonic Bandgap Fibers," Opt. Express **12**, 4080 (2004).
21. H. P. Kao, N. Yang, and J. S. Schoeniger, "Enhancement of Evanescent Fluorescence from Fiber-Optic Sensors by Thin-Film Sol-Gel Coating," J. Opt. Soc. Am. A **15**, 21632,170 (1998).
22. M. Nagel, A. Marchewka, and H. Kurz, "Low-Index Discontinuity Terahertz Waveguides," Opt. Express **14**, 9944 (2006).
23. G. S. Wiederhecker, C. M. B. Cordeiro, F. Couny, F. Benabid, S. A. Maier, J. C. Knight, C. H. B. Cruz, and H. L. Fragnito, "Field Enhancement Within an Optical Fibre with a Subwavelength Air Core," Nature Photonics **1**, 115 (2007).
24. N. Ganesh and B. T. Cunningham, "Photonic Crystal Enhanced Fluorescence," in *Technical Digest*, p. CThz5 (Optical Society of America, 2007).
25. V. R. Almeida, Q. Xu, C. A. Barrios, and M. Lipson, "Guiding and Confining Light in Void Nanostructure," Opt. Lett. **29**, 1209–1211 (2004).
26. R. E. Bailey, A. M. Smith, and S. Nie, "Quantum Dots in Biology and Medicine," Physica E **25**, 1–12 (2004).
27. A. W. Snyder and J. D. Love, *Optical Waveguide Theory* (Chapman and hall, 2-6 Boundary Row, London SE1 8HN, UK, 1995).
28. F. W. D. Rost, *Fluorescence Microscopy* (Cambridge University Press, Cambridge, UK, 1992).
29. D. Marcuse, "Launching Light Into Fiber Cores from Sources Located in the Cladding," J. Lightwave Technol. **6**, 1273–1279 (1988).
30. H. Ebendorff-Heidepriem, P. Petropoulos, S. Asimakis, V. Finazzi, R. C. Moore, K. Frampton, F. Koizumi, D. J. Richardson, and T. M. Monro, "Bismuth Glass Holey Fibers with High Nonlinearity," Opt. Express **12**, 5082–87 (2004).
31. C. M. B. Cordeiro, M. A. R. Franco, C. J. S. Matos, F. Sircilli, V. A. Serrao, and C. H. B. Cruz, "Single-Design-Parameter Microstructured Optical Fiber for Chromatic Dispersion Tailoring and Evanescent Field Enhancement," Opt. Lett. **32**, 3324–26 (2007).
32. A. Zheltikov, "Gaussian-Mode Analysis of Waveguide-Enhanced Kerr-Type Nonlinearity of Optical Fibers and Photonic Wires," J. Opt. Soc. Am. B **22**, 1100–1104 (2005).
33. P. Agrawal, *Nonlinear Fiber Optics*. Academic press, Burlington, (2007).
34. E. W. Washburn, "The Dynamics of Capillary Flow," Physical Review **17**, 273–283 (1921).
35. I. B. Berlman, *Handbook of fluorescence spectra of aromatic molecules* (Academic Press, New York, 1971).
36. E. Schartner, Y. Ruan, P. Hoffman, and T. M. Monro, "An Optical Fibre Protein Sensor," in *COIN-ACOFT 2007 Proceeding*, pp. WeB1–3 (Australian Optical Society, 2007).
37. Y. Ruan, W. Li, R. Jarvis, N. Madsen, A. Rode, and B. Luther-Davies, " Fabrication and Characterization of Low Loss Rib Chalcogenide Waveguide Made by Dry Etching, " Opt. Express **12**, 5140–5145(2004).
38. H. Ebendorff-Heidepriem, Y. Li, and T. M. Monro, "Reduced Loss in Extruded Microstructured Optical Fiber," Electron. Lett., **43**, 1343–1345(2007).

1. Introduction

Microstructured optical fibres (MOFs) have the potential to dramatically improve the performance of fibre optic sensors based on absorption and fluorescence spectroscopy and have recently attracted considerable interest [1, 2, 3, 4, 5, 6, 7], since a significant portion of the guided light can be located in holes within the fibre. In the literature, the sensitivity of optical fibre sensors based on absorption and fluorescence spectroscopy is usually considered to be related solely to the power fraction of the guided mode field that is available for overlap with the ma-

terial to be sensed. Such sensors are generally referred to as evanescent-field sensors, reflecting the fact that only the evanescent tail of the guided mode is available for light-matter interactions. Examples of fibre geometries used for evanescent-based sensing include; tapered fibres [8, 9], D-shaped fibres [10], optical nanowires [11], solid-core MOFs [5, 12], multi-core MOFs [3, 4] and hollow-core MOFs [13]. Most evanescent-based sensing geometries only allow a limited light-matter overlap and thus are restricted in the sensitivity that they can achieve. Some typical mode-matter overlaps that have been reported include $0.1 - 0.2\%$ for D-shaped fibres [10], 5.2% in an MOF [13], and multi-core MOFs with 6.5% [4]. Fibres with sub-wavelength cores including optical nanowires and MOFs with embedded nanowire-like cores [14, 15] allow overlaps as large as 99% as is evident from literature reports of 40% [12] and 99% [16]. These advances allow solid-core fibres to achieve light-matter overlaps as high as other field-based sensors which have access of up to 97% [17] or higher of the guided mode power such as capillary tubes [18], index-guiding filled hollow-core MOFs [19] and hollow-core photonic band gap fibres [20].

Although different MOF-variants of fluorescence-based sensors have been reported [2, 3, 4, 7, 10], the benefits that can be obtained using MOFs are far from being realised, largely due to the lack of a formalism for predicting and thus optimizing the measurable fluorescence power. Although models of the efficiency of fluorescence-based optical fibre sensors have been developed for simple structures such as tapered or D-shaped fibres, they have limited applicability because; 1) it is assumed that the modes of the fibre are the same at both the absorption and fluorescence wavelengths and 2) they are based on ray-optics [1, 21] or scalar electromagnetic fields (without including the effect of absorption loss) [8]. These models do not work well for fluorescent dyes with significant excitation-fluorescence wavelength separation (such as quantum dots), MOFs with wavelength-scale features and high contrast refractive indices, or complex sensing geometries when the hole surface of MOFs are coated (functionalized) with chemical-biological materials.

Here, we develop a general model of excitation and fluorescence recapturing within an MOF's modes based on guided mode solutions of vectorial form of Maxwell's equations and considering their losses at both emission and fluorescent frequencies. By evaluating the modal characteristics of a range of fibres at both wavelengths, we explore ways of enhancing the sensing sensitivity by maximising the fraction of the fluorescent photons that are coupled to the guided mode(s) of the filled microstructured fibres (the fluorescence capture fraction, FCF). We demonstrate that the light-matter overlap alone does not determine the optimal fibre choice as is usually assumed. Fibre designs with sub-wavelength features and high index glass exhibit localised regions of high intensity [22, 23], and we show that these regions lead to enhanced fluorescence recapturing and can be exploited for sensing. The significance of this parameter regime becomes clearer considering; 1) recent indication of the existence of such narrow-width high intensity regions at the interface of two different dielectrics, due to discontinuity of the electric field, in both waveguides [25] and MOFs [22, 23] and 2) sensing configurations based on surface excitation of chemical and biological layers. Recently, there have been reports on the importance of the above-mentioned parameter regime in related fields. The enhancement of fluorescent scattering of semiconductor quantum dots deposited upon photonic crystals slabs [24] and the enhancement (by few orders of magnitude) of the efficiencies of conventional surface spectroscopy by using tapered fibres [6] are two examples.

Experimentally, chemical and biological sensing have been demonstrated using absorption spectroscopy in D-shaped fibres [10] and MOFs [4, 5] and captured fluorescence-based sensing in tapered fibres [26], liquid-filled hollow-core MOFs [19, 7], side excited MOFs [2, 17], and double-clad and multi-core (liquid filled) MOF [3]. Here, we demonstrate experimentally both in-fibre excitation and fluorescence recapturing within a liquid-filled, solid-core, index-guiding

MOF [Fig. 1(b)] through its core guided modes. The experimental methods based on selective hole filling of MOFs (c.f. Ref. [19, 7] for example) or propagating modes of high index liquids (c.f. Ref. [3] for example) may be limiting in some applications. Thus, the use of high-index glass (SF57 here) solid-core MOFs allows access to high light-matter overlaps without necessitating selective hole filling while relying on solid-core modes even when the MOF holes are filled with high index liquid.

2. Theory

To develop the model, we assume that the propagating modes of an absorbing MOF are the same as nonabsorbing ones except that their powers decay with an attenuation factor of γ as they propagate. The excitation electromagnetic power in the jth mode at excitation frequency ω_E can then be expressed as: [27]

$$P_{Ej}(z) = \left|a_{Ej}\right|^2 N_{Ej} \exp(-\gamma_{Ej} z); \quad N_{Ej} = \frac{1}{2}\mathrm{Re}\left\{\int_{A_\infty} (\mathbf{e}_{Ej} \times \mathbf{h}^*_{Ej}).\hat{z} dA]\right\} \tag{1}$$

$$\gamma_{Ej} = k\left(\frac{\varepsilon_0}{\mu_0}\right)^{1/2} \frac{\int_{A_\infty} n_E n_E^i \left|\mathbf{e}_{Ej}\right|^2 dA}{N_{Ej}}, \tag{2}$$

where a_{Ej} is the expansion coefficient for mode j, $\mathbf{e}_{Ej}(x,y), \mathbf{h}_{Ej}(x,y)$, β_{Ej}, and γ_{Ej} are the j^{th} mode electric and magnetic field distributions, propagation constant and power decaying factor due to absorption, respectively. Here, we assume that γ_j represents all absorption mechanisms in the MOF, including absorption due to the Beer-Lambert law [28].

For an arbitrary filled MOF both $n_E(x,y)$ and $n_E^i(x,y)$ (real and imaginary parts of refractive indices) are functions of transverse coordinates and hence the piece-wise integral in Eq. (2) can be integrated over the glass and hole (filled) regions. Eq. (1) indicates that although the absorption of the excitation mode occurs in the filled region, through Beer-Lambert law, the peak intensity also reduces, keeping the shape of the mode and the hole power fraction constant.

Upon absorbing the excitation photons, the fluorescent species in the holes behave as sources and emit fluorescent photons in all directions. Similar to the excitation field, the emission of this new fluorescent source can in general be written [27] as the sum of forward, backward, and radiation modes of the non-absorbing MOF with the consideration of power decay due to loss at the fluorescence frequency. Based on the formalisms developed in Ref. [27, 29], we find the fluorescent power contribution to the jth forward mode of the MOF at the end of the filled region $z = L$, due to a small section $\Delta z = z_2 - z_1$ [see Fig. 1(c)], and including its loss as:

$$dP_{Fj}(z') = \frac{\pi \exp[-\gamma_{Fj}(L-z')]}{4\omega_F \mu_0 n_F^H k_F N_{Fj}} \int_H \int_{z_1}^{z_2} \left|\mathbf{e}_{Fj}\right|^2 P_D(\mathbf{r}) dz'' dA. \tag{3}$$

Here, $P_D(\mathbf{r})$ is the radiation power density of any sources within the MOF, which for the case considered here is due to the fluorescent emission of the filling material. The density of fluorescent emission at point $\mathbf{r}$ depends on the absorption of excitation field from the beginning of the filled area up to the point $\mathbf{r}$, see Fig. 1(a). Using equations (1) and (2), assuming that the fluorescent power density is proportional to the density of excitation power loss due to Beer-Lambert law in the filled region (proportionality constant ξ), and taking into account energy conservation, we have found $P_D(\mathbf{r})$ as:

$$P_D(\mathbf{r}) = \frac{1}{2}\xi \alpha_B n_E^H (\varepsilon_0/\mu_0)^{1/2} \left|a_{Ej}\right|^2 \delta_{Ej}^H \mathrm{Re}[(\mathbf{e}_{Ej} \times \mathbf{h}^*_{Ej}).\hat{z}] \exp(-\gamma_{Ej} z''), \tag{4}$$

$$\delta_{Ej}^H = \int_H \left|\mathbf{e}_{Ej}\right|^2 dA / \int_H (\mathbf{e}_{Ej} \times \mathbf{h}^*_{Ej}).\hat{z} dA. \tag{5}$$

Here, $\alpha_B = \varepsilon_\lambda C$ is the absorption coefficient due to Beer-Lambert law [28], where ε is the molar extinction coefficient of the filling material, C is the molar concentration, and superscript H refers to hole regions. Substituting Eq. (4) into Eq. (3), and taking the integral over z'' and the limit of $z_1 \to z_2$, we find

$$dP_{Fj}(z') = \frac{\pi\xi\,\alpha_B n_E^H (\varepsilon_0/\mu_0)^{1/2} \left|a_{Ej}\right|^2 \delta_{Ej}^H}{8\omega_F \mu_0 n_F^H k_F N_{Fj}} \exp[-\gamma_{Fj}(L-z')]\exp(-\gamma_{Ej}z')dz' \times \int_H \left|\mathbf{e}_{Fj}\right|^2 \mathrm{Re}[(\mathbf{e}_{Ej}\times\mathbf{h}_{Ej}^*).\hat{z}]dA. \tag{6}$$

Integrating the fluorescent contributions of the elements from $z = 0$ to $z = L$, the fluorescence capture fraction (FCF) into the jth guided mode of the MOF can be expressed as

$$FCF = P_{Fj}(L)/P_{Ej}(0) = AB_j \frac{\exp(-\gamma_{Fj}L)}{(\gamma_{Ej}-\gamma_{Fj})}\{1-\exp[(\gamma_{Fj}-\gamma_{Ej})L]\} \tag{7}$$

$$A = \frac{\xi\,\alpha_B\lambda^2}{8\pi(n_F^H)^2}; \quad B_j = n_F^H n_E^H \left(\frac{\varepsilon_0}{\mu_0}\right)\delta_{Ej}^H \frac{\int_H \left|\mathbf{e}_{Fj}\right|^2 \mathrm{Re}[(\mathbf{e}_{Ej}\times\mathbf{h}_{Ej}^*).\hat{z}]dA}{4N_{Fj}N_{Ej}}. \tag{8}$$

In this equation A is a constant coefficient and $P_{Ej}(0)$ is the input excitation field power at the beginning of the filled part of the fibre, whose length is shown by L [see Fig. 1(a)]. It should be noted that throughout the text we only consider FCF into the fundamental guided mode propagating in the forward direction. To find FCF into backward propagating modes, different loss calculations should be included in the above formalism which is beyond the scope of this paper. Also, in derivation of Eq. (6) and (7), it is assumed that the whole fibre length is completely filled. For fibres that are only partially filled, the mode mismatch between the filled and unfilled sections should be considered for both excitation and fluorescence frequencies, which is beyond the scope of this paper.

3. Modelling results and discussion

The model developed in Section 2 is general and can be applied to any filled MOF with arbitrary cross section structure. Here, we consider an MOF [shown in Fig. 1(b)], which consists of a core surrounded by three large, non-circular, air holes creating a somewhat triangular core supported by three struts. This type of fibre geometry has been studied [30, 31] and is the simplest fibre geometry that can be fabricated giving rise to a well defined air-suspended core with large surrounding (fillable) air holes. To find the propagation constant and field distributions for the MOF, we solve the full vectorial form of Maxwell's equations since, for the subwavelength scales considered here, a scalar approximation gives inaccurate results [32].

We define the MOF core diameter, d, to be the diameter of a circle with area equal to that of the largest equilateral triangle that fits wholly within the substrate core region, shown as the solid circle in Fig. 1(b). For simplicity we consider an idealized MOF structure, which closely matches that of the SEM image [Fig. 1(b)]: the curvature of the core is approximated by the edges of the three dashed circles connected by the bases of three rectangles approximating the struts. To solve Maxwell's equations for this geometry we use the Finite Element Modelling (FEM) technique instantiated in the commercial FEM package COMSOL 3.2. The accuracy of the modal parameters depends heavily on the densities of the mesh in different regions, which have been set separately to achieve converged values. The parameters used for the simulations are; excitation wavelength $\lambda_E = 532\ nm$, fluorescence wavelength $\lambda_F = 590\ nm$, filling material: Rhodamine B dissolved in isopropanol, and five different glass materials [silica, lead silicates (LLF1, F2, and SF57), and bismuth] whose refractive indices are indicated on the figures.

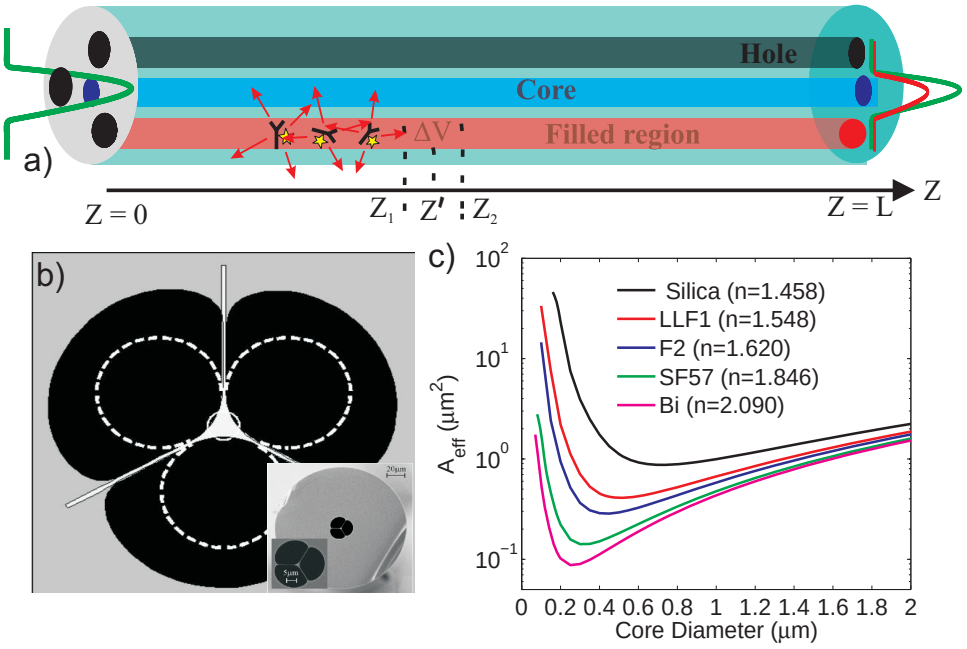

Fig. 1. Schematic of a filled MOF showing the parameters used in modelling (a) and the SEM image of the cross section of the MOF used for the modelling and experiment (b). Dashed circles in (b) show the idealized geometry used for modelling. The effective area of the fundamental mode for the geometry shown in (b) when the holes are filled with Rhodamine B in an isopropanol solution (c). The wavelength is 590 *nm*, refractive index of isopropanol is 1.3774 and different substrate glasses are marked.

Simulation results of FCF as a function of fibre length for constant core diameter and concentration, as shown in Fig. 2(a), indicate that there is an optimum fibre length $L_{opt} = \ln(\gamma_F/\gamma_E)/(\gamma_F - \gamma_E)$, which leads to maximal FCF for any fibre geometry [see Eq. (7)]. For $L < L_{opt}$ increasing the fibre length increases the absorption in the filled region via the Beer-Lambert law, and thus increases FCF. Beyond this optimum length, fibre attenuation dominates and the fluorescent power decays as $\exp(-\gamma_F L)$. Unsurprisingly, as the results in Fig. 2(a) show, the use of lower index glasses results in a higher FCF since the relatively low core-cladding index contrast leads to a higher light-matter overlap within the holes [this is also evident in the behaviour of A_{eff} in Fig. 1(c)].

Numerical simulations of the FCF also identify a less obvious and particularly interesting regime [see Fig. 2(b)]. For small core diameters ($d < 0.8\ \mu m$), the FCF can be significantly enhanced by employing high index (soft) glasses. For example, the maximum FCF (FCF at fibre length L_{opt}) for bismuth-oxide fibres at $d \approx 0.18\ \mu m$, is 2.2%, 10 times larger than the maximum FCF value for silica fibres (0.22%) at $d \approx 0.52\ \mu m$. Also, at the core size of $d \approx 0.2\ \mu m$ the maximum FCF value for bismuth fibres is 2.1%, 88 times larger than that of silica fibres (0.024%). This is contradictory to the usual assumption that sensitivity is proportional to power fraction in the holes, since high index glasses result in lower power fraction in the holes compare to that of low index glasses at small core diameter. For example, at the core diameter of $d \approx 0.2\ \mu m$ hole power fraction at excitation frequency (defined as $\eta_E^H = n_E^H (\varepsilon_0/\mu_0)^{1/2} (1/2N_{Ej}) \int_H |\mathbf{e}_{Ej}|^2 dA$) for silica and bismuth fibres are 0.97 and 0.43 re-

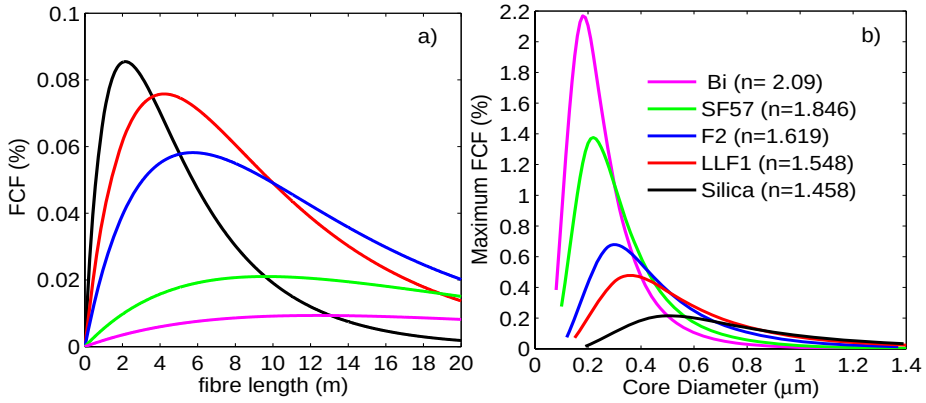

Fig. 2. Numerical results of the fluorescence capture fraction (FCF) as a function of fibre length (a) and core diameter (b) for different substrate glasses. Other parameters are; core diameter 1.0 μm, in (a) and concentration 5×10^{-5} Mol in (a) and (b). Maximum FCF in (b) corresponds to optimum fibre length.

spectively.

To understand this effect, we examine coefficient B_j in Eq. (8), which depends on the field distributions of the guided modes of the fibre and their overlap with the materials within the holes. We assume that the mode profiles of the excited and fluorescent fields are the same (i.e., $N_{Fj}=N_{Ej}$), which although not strictly true especially for filling materials such as quantum dots with large separation of absorbing and fluorescent wavelengths, can help provide physical insight. We rewrite coefficient B_j as $B_j = NOI_j/A_{eff}$, where;

$$NOI_j = n_E^H n_F^H \left(\frac{\varepsilon_0}{\mu_0}\right)^{1/2} \frac{\delta_{Ej}^H \int_H \left|\mathbf{e}_j\right|^2 \mathrm{Re}[(\mathbf{e}_j\times\mathbf{h}_j^*).\hat{z}]dA}{\int_{A_\infty}\left|\mathrm{Re}[(\mathbf{e}_j\times h_j^*).\hat{z}]\right|^2 dA}; \quad A_{eff} = \frac{(\int_{A_\infty}\mathrm{Re}[(\mathbf{e}_j\times h_j^*).\hat{z}dA])^2}{\int_{A_\infty}\left|\mathrm{Re}[(\mathbf{e}_j\times h_j^*).\hat{z}]\right|^2 dA}.$$

Here NOI_j is a normalized field-matter overlap integral, which approaches 1 when the core diameter becomes very small and most of the light is located outside the core [see Fig. 3(a)]. A_{eff} , defined based on z component of the Poynting vector, is a generalised form of the usual definition of A_{eff} [33].

Inspecting A_{eff} [Fig. 1(c)] and NOI [Fig. 3(a)] at a core size of $d = 0.2$ μm for both silica and bismuth, reveals that the field-matter overlap NOI for silica is 3.6 times larger than that of bismuth. However the effective area, A_{eff}, of the propagating mode for bismuth is 230 times smaller than that of silica for this core diameter, resulting in higher intensity values for bismuth and thus a larger FCF. Examining the intensity profiles of the fundamental mode for these silica and bismuth fibres [Fig. (4)], clearly shows that while the mode is well expanded into the hole region in the case of silica, it is well confined within the core for bismuth and forms a high intensity, thin layer at the core-hole interface within the filled region.

These localised high intensity regions are formed due to the discontinuity of the electric field at the interface of two dielectric media, as recently reported in slab waveguides [25] and MOFs [22, 23]. The magnitude of the discontinuity is proportional to the ratio of the dielectric

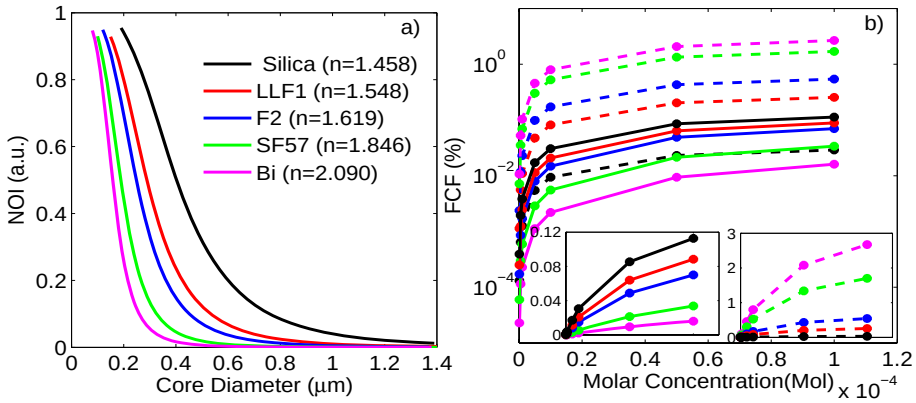

Fig. 3. Numerical results of Normalized Overlap Integral (NOI), defined in the text and calculated at the wavelength of 590 *nm* (a), and the fluorescent capture fraction (FCF) as a function concentration (b). In (b) dashed and solid lines correspond to core diameters 0.2 and 1.0 μm respectively, and the insets show the linear scale plot of the main graph over the same concentration range.

constants of the two media and hence soft glasses with higher refractive indices result in higher intensities at the glass-hole interface.

The results presented here demonstrate for the first time that overlapping localised high intensity regions in the modal field with a fluorescent material is an effective way of enhancing the performance of a sensing fibre. This enhancement is significant not only for situations where the holes are filled with liquids, but is also particularly relevant for sensing configurations where samples are coated or functionalized onto the walls of the MOF. This enhanced *FCF* regime,

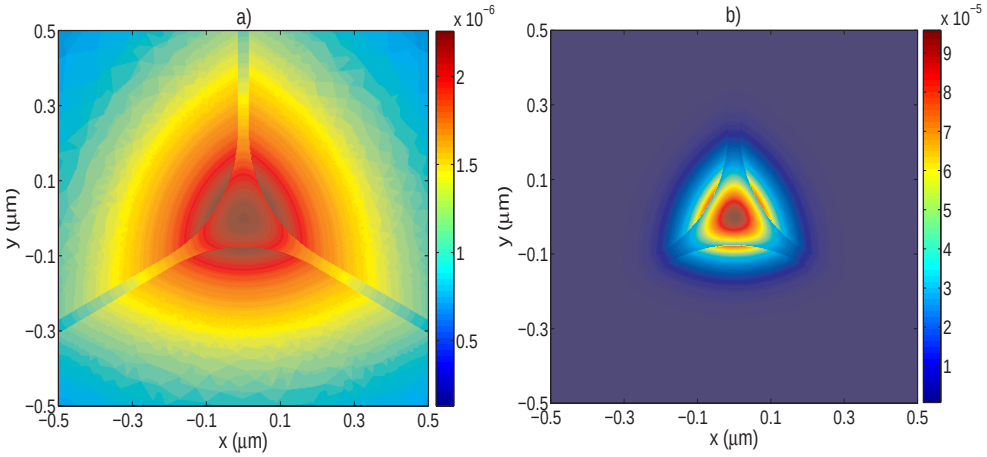

Fig. 4. Intensity distribution of the fundamental mode for Silica (a) and Bismuth (b). In both (a) and (b) core diameters are 0.2 μm and the wavelengths are 590 *nm*. The mode is more confined in (b) and a thin layer of high intensity region is formed at the glass-hole interface.

achieved by the use of small core dimensions and high index glasses, also enhances the sensitivity of FCF to concentration variations in the material to be sensed. Using Eq. (7), the FCF can be approximated as $[1-\exp(-\varepsilon_\lambda C\eta_{Ej}^H)]$ as a function of concentration C, which simplifies to $\varepsilon_\lambda C\eta_{Ej}^H$ in the limit of small concentration. This behaviour of FCF is confirmed as shown in Fig. 3(b) for two core diameters $d = 1.0$ (solid lines) and $d = 0.2\ \mu m$ (dashed lines) and different glasses. However, the behaviour of FCF as a function of concentration C is opposite for small and large core regimes. Fig. 3(b) and its insets show that for large core diameters (e.g., $d = 1.0\ \mu m$), silica has the largest asymptotic FCF value ($\sim 0.11\%$) and FCF slope ($\partial(FCF)/\partial C \sim 0.0027\%/\mu M$). Whereas, for small core diameter ($d = 0.2\ \mu m$), bismuth has the largest corresponding FCF value of (~ 2.67) and FCF slope ($\sim 0.069\%/\mu M$). As a result, both FCF and its sensitivity to small variations in concentration are enhanced in the small core, high index glass regime. This regime is expected to be of particular practical benefit in allowing observations of captured fluorescence to occur at extremely low sample concentrations, allowing for the development of sensors with competitive detection limits.

4. Experimental results

We have demonstrated experimentally in-fibre excitation and fluorescence recapturing within a filled, solid-core MOF. The holes of the MOF, shown in Fig. 1(b), were filled with Rhodamine B dissolved in isopropanol ($n = 1.3774$) using capillary action. Using the experimental setup in Fig. 5(a), Fig. 5(b) shows the experimental measurements and theoretical prediction of the filling rate. We use the filling rate equation developed in Ref. [34] for a circular capillary tube, considering the following parameters for isopropanol, its interaction with glass, and the fibre geometry; density 785 kgm^{-3}, surface tension 0.022 Nm^{-1}, viscosity $2.27\times10^{-3}\ Nsm^{-2}$, effective radius $6.11\times10^{-6}\ m$, contact angle 0°, coefficient of slip 0 m, and external pressure 0 Pa. To find the effective radius r_{eff}, we have assumed that the holes of the MOF in Fig. 1(b) are circular with the same area as that of the real fibre. This, strictly speaking, is inaccurate because capillary forces are mainly a surface effect, which depends on the radius of curvature of the different corners in the geometry, and we believe that this assumption is the main reason for the discrepancy between the theoretical and experimental results in Fig. 5(b). For these experimental measurements the position of the liquid in the holes was recorded by observing the fluorescent emission at the liquid interface in the backward direction of the laser beam in Fig. 5(a).

The setup sketched in Fig. 5(c) was used to excite the Rhodamine B molecules filled into the holes of the fibre and measure the captured fluorescence emission. The outer surface of the fibre was coated with an index matching liquid, DAG, to strip any fluorescent emission coupled to the cladding modes. This ensured that all the measured fluorescence had been captured by the relatively low-loss, core-guided modes of the fibre, as assumed by the theoretical model. The absorption and low concentration fluorescent peaks of Rhodamine B are at 540 nm [35] and 570 nm, respectively. The MOF used in the experiment has a core diameter of $d = 1.8\ \mu m$, core material of SF57 and its cross section is shown in Fig. 1(b). A CW laser at 532 nm was coupled into the MOF using an aspheric lens of $f = 2.75\ mm$ and $NA = 0.65$ and maximum coupling efficiency of around 19% was measured. The loss of the unfilled fibre at 532 nm is $5.5\pm0.5\ dB/m$, using the standard cutback method. At the output, we used a long pass filter to exclude the excitation frequency components. The fluorescence emission is then coupled into a single mode (SM) fibre, which was connected to an optical spectrum analyser for spectrum measurement.

The experimental results are presented in Fig. 5(d) clearly showing the expected fluorescence and also significant decay of the measured fluorescence over 960 seconds exposure to the excitation field. The decay in fluorescence was due to photobleaching, the photo-induced

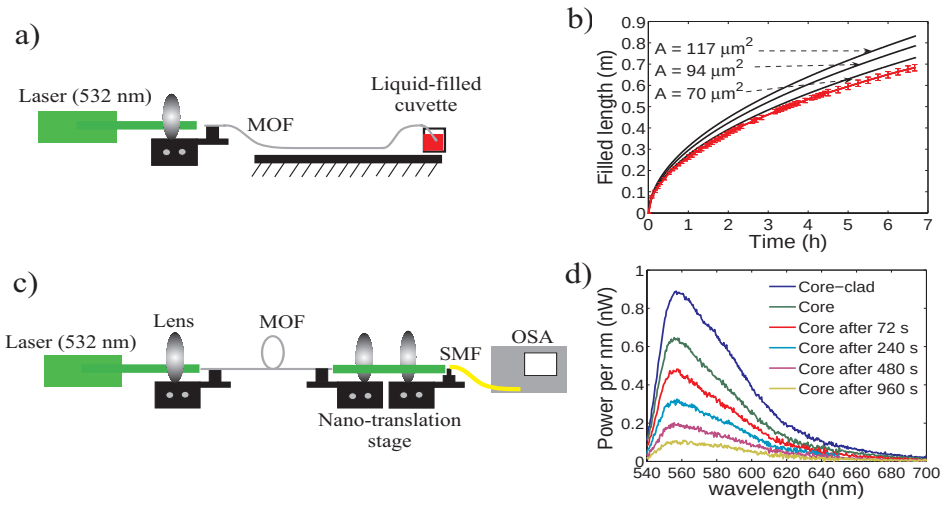

Fig. 5. Experimental setup for filling an MOF (a). The experimental and theoretical predications of filling time as a function of filled length (b). For the theoretical predictions it is assumed that the holes of the fibre are circles whose area are 1, 0.8, or 0.6 times of that of the real fibre in Fig. 1 (117, 94, and 70 μm^2 respectively). Experimental set up (c) and results (d) for capturing the fluorescent emission by the core of the MOF.

destruction of the fluorophore [28]. While partial recovery is possible, photobleaching has the potential to be problematic. For example, to measure FCF as a function of fibre length we fill a fibre and use a cut-back method to measure FCF at different lengths. However due to photobleaching effect and the time that takes to cleave, align, and couple the fluorescence beam into the OSA, it is very difficult to measure FCF as a function of length for Rhodamine B. A promising alternative is to replace organic dyes with quantum dots, which experience negligible photobleaching and have already found use in sensing such as for biological and medical applications [26, 36].

5. Discussion and conclusion

To the best of our knowledge this is the first time that a general model of both in-fibre excitation and fluorescence recapturing of filled solid-core MOFs by their core guided modes has been developed and demonstrated experimentally. An expression for the efficiency of fluorescence capture fraction has been developed for an arbitrary MOF based on vectorial solutions of Maxwell's equations and considering the modal behaviour of the MOF for distinct excitation and fluorescence frequencies. We have predicted between one to two orders of magnitude improvement in the fluorescence capture fraction (FCF) of MOFs with high index substrate glasses and small core diameters in comparison with those with low index glasses. This parameter regime results in localised, high intensity electromagnetic fields at the interface of the glass and hole regions, making it an ideal regime for thin layer sensing where chemical or biological substances are coated onto the interface.

The fluorescence capture fraction is normalised to the input power in the fibre and hence, although the small core parameter regime degrades the coupling efficiency, higher incident power (below the damage threshold of the glass) can be used to attain certain power in the fibre. Additionally, by using advanced coupling techniques such as tapers or high numerical aperture buffer fibres [37], one should be able to minimise the coupling loss into small core

fibres.

Our recent progress in fabricating soft glass MOFs with small cores, and the evidence that with careful fabrication processes fibre loss of order of $< 0.5\ dB/m$ can be achieved [38], provide an attractive new route towards the development of highly-sensitive fluorescence sensors.

Acknowledgements

We acknowledge the Defence Science and Technology Organization (DSTO), Australia, for supporting research in the Centre of Expertise in Photonics. We would also like to acknowledge the help and expertise of Dr Heike Ebendorff-Heidepriem with topics in glass chemistry and extrusion, Mr. John Debs with fibre filling experiments, and Mr. Roger Moore with fibre drawing.